IEEE Access
Multidisciplinary | Rapid Review | Open Access Journal

Received June 19, 2021, accepted July 5, 2021, date of publication July 26, 2021, date of current version August 31, 2021.

Digital Object Identifier 10.1109/ACCESS.2021.3099425

Equidistributed Search+Probability Based Tracking Strategy to Locate an Air Pollutant Source With Two UAVs

ANDRÉS F. GARCÍA-CALLE[1], LUIS E. GARZA-CASTAÑÓN[1], (Member, IEEE), AND LUIS I. MINCHALA-AVILA[2], (Senior Member, IEEE)

[1]School of Engineering and Sciences, Tecnologico de Monterrey, Monterrey, Nuevo León 64849, Mexico
[2]School of Engineering and Sciences, Tecnologico de Monterrey, Guadalajara, Jalisco 45201, Mexico

Corresponding author: Luis E. Garza-Castañón (legarza@tec.mx)

This work was supported in part by Consejo Nacional de Ciencia y Tecnologia (CONACYT), Mexico, and in part by the Tecnologico de Monterrey.

ABSTRACT As the atmospheric pollution becomes an increasingly serious problem, finding accurately the location of pollutant sources is still challenging. In the present work, a probability-based tracking strategy is proposed for guiding two cooperative unmanned aerial vehicles (UAVs) within a quest area to find an atmospheric pollutant source. This tracking strategy implies deploying algorithmically two phases: exploration and exploitation. During the exploration phase each vehicle follows a trajectory based on plane coordinates generated from a Hammersley sequence. The overlapping between UAVs' trajectories is avoided by splitting guidance points into two groups by using the k-means algorithm. The navigation trajectories are smoothed by an TSP solver and a cubic spline planning algorithm. The exploitation phase redirects the search to specific locations where the probability of finding the source is higher. This is achieved by considering the quest area as a mesh, where each cell is assigned a probability computed with information collected by the UAVs measurement system. Every time a high concentration is found, the probabilities are recalculated, and flight trajectories are adjusted. The trajectories are semicircular, and the radius is decreased when a new high concentration is found. Simulation data of the proposed tracking strategy shows promising results on the accuracy achieved in the finding of the pollutant source, in comparison with three other tracking strategies: leader-follower, random walk with particle swarm optimization, and a hill climb traceability algorithm.

INDEX TERMS Air pollution, aircraft navigation, source localization, time-varying source, unmanned aerial vehicles.

I. INTRODUCTION

There are many areas in which unmanned aerial vehicles are helpful to accomplish complex or risky tasks. For instance, applications related to civil structures monitoring, mapping of urban and natural areas, search and rescue in emergency scenarios, and environmental monitoring. Nowadays, there are increasingly better efforts in research and development for using UAVs to locate and identify pollutant sources. A source could be radiation, acoustic signals, electromagnetic signals, or a chemical agent. This paper contributes in this specific area. The main purpose is locating an air pollutant source on an outdoor scenario by considering realistic time constraints related to the UAVs battery. This task is accomplished by a couple of autonomous quadcopters equipped with appropriate sensors which measure a specific pollutant. UAVs can move with 6 degrees of freedom and are capable to fly for a limited time in different environments, making them suitable to take pollutant samples.

Up to date literature reports several applications of UAVs for locating pollutant sources. For instance, [1]–[6] use multiple mobile robots to sample their search area. In these works, global optimization algorithms command the movement of each robot. Reference [1] details a leading-follower strategy by using a PSO algorithm for guiding the mobile robots. Each robot is considered as a particle of the swarm and the Schrödinger equation guides the movement. The leader of the swarm is chosen depending on the global optimal position. The followers serve the leader providing measurements and navigating in the direction chosen by the leader. The authors

The associate editor coordinating the review of this manuscript and approving it for publication was Juan Liu.

of [2] use an indoor controlled environment to perform source tracking. Two experiments are developed in this work: one of them considers airflow information, while the other does not consider airflow information. The airflow is varied with displacement ventilation or mixing ventilation. For each experiment six terrestrial robots are guided in 3 phases: finding the plume (with a random divergence strategy), tracking the plume (by a standard and improved Whale Optimization Algorithm), and declaring the source.

In a platform with multiple agents, cooperation is a powerful tool to succeed in the task of finding a source. Research reports in [7]–[10] focus on reducing their time to accomplish a mission and exchange information between each robotic agent. In [7] the agents share their position, velocity, and formation vector to perform a coordinated scanning of the search area. There are four UAV agents in this approach. The exploration phase carries out three strategies: leader-follower, random walk scanning with feasible drone orientations, and Brownian motion behavior. The exploration phase performs the following steps:

1) The UAV that reacts to a gas measurement is transformed into a leader
2) A circular formation around the leader is performed
3) The swarm moves along a logarithmic spiral
4) If the *i*-th UAV detects a gas concentration, greater than previous measures, that UAV is considered the new leader

The plume is simulated with a Gaussian model, and the experiments assume that the gas concentration is a decreasing function of the distance from the source.

Previous strategies were proved in simulated environments or indoor controlled experiments. However, in the literature is possible to find several works implemented in outdoor scenarios [9], [11]–[13]. In these works, the focus is made on the construction of a platform with high maneuverability and capacity to sense air pollutant concentrations. With those platforms, it is possible to execute exploratory and exploitative strategies for source tracking. Different pollutant sources have been considered in research works, such as sources of alcohol [14], sound [15], or even it is considered to fly in zones where the presence of contamination is known [16]–[18]. It is common to find articles that use potential fields to implement the collision avoidance [19]–[22]. To the best knowledge of the authors of this research work, some papers report applications similar to our approach. Nevertheless, several assumptions (for simulation works) or favorable initial conditions (for experimental approaches) are considered in these works. Some examples of these favorable factors are as follows:

- Take-offs from inside a plume, [19], [23] or relatively close to it [24]
- The initial fly direction is towards the plume [19], [20]. These conditions oversimplify the problem of finding first clues
- The carried sensors have a high sensitivity [25]. This implies the use of expensive sensors
- The search area is not extensive, so UAVs can detect the plume before flight time runs out [21]. In other words, UAVs can easily cover the entire area before they run out of power

This paper presents results on the application of a novel intelligent strategy to locate an air pollutant source, without any favorable environmental conditions, as the previously described in [19]–[21], [23]–[25]. Main considerations of this work include:

- A platform with two UAVs, although using more units is possible with minor modifications to the strategy
- Take-offs in zones where there is not a minimal trace of the pollutant plume. This requires the implementation of a fast coordinated exploration phase
- Path planning depends on clustering deterministic points, but with random initial centroids (with k-means)
- Parameters like maximum ground speed, the sensitivity of sensors, flying time, radio frequency coverage area, among others, are more constrained and selected according to similar UAVs used in the work proposed by [13]
- The search area is large enough (500m $\times$ 500m). The ratio of area covered by the plume and the total search area is less than 3/100

Another important feature of our work is that we use real measurements of wind magnitude to simulate the pollutant plume. The simulation environment uses the MAVLINK navigation protocol [26]. The main objectives of these features are: to simulate a wind behavior closer to reality, and to allow a simple migration of the developed scripts to a real platform (similar to the used in [13]).

The performance efficiency of the UAVs to track and locate an air pollutant source is performed. To this purpose, parameters like distance to the source, time to finish the exploration phase, highest pollution measure taken, and ability to detect higher contaminant measurements will be statistically analyzed.

Four different strategies for the exploration phase, each accompanied with its respective strategy for the exploitation phase, are tested in a scenario with a simulated pollutant plume. To avoid collisions between the UAVs, they fly at different heights like in [27]. These heights remain constant during flight time. In half of the experiments the height of one UAV matches with the pollutant source height. In the rest of the experiments no UAV matches with the source height.

The main content of this paper is organized as follows: section 2 describes the simulation environment and the air pollutant distribution model, the construction of a probabilistic map, and the explanation of strategies. Section 3 presents the results obtained in experiments and the analysis. Section 4 presents the conclusions and future work.

II. SEARCH AREA MODELING THROUGH PROBABILISTIC REFERENCE MAP

A. POLLUTANT PLUME MODELING

To analyze the polluting plume model, is necessary to consider two phenomena: the contaminant diffusion into the

atmosphere and the movement of these diffused concentrations due to the wind [28]. These behaviors correspond to the equation of concentration given by:

$$\frac{\partial c}{\partial t} + \nabla \cdot \vec{f} = s \tag{1}$$

where:

- $c(\vec{X}, t)$ is the concentration of the pollutant mass in a given time $t[sec]$ and position $\vec{X} = (x, y, z) \in \mathbb{R}[m]$.
- $s(\vec{X}, t)$ is the source of contamination.
- $\vec{f}(\vec{X}, t)$ is the flow of contaminant mass due to diffusion and advection phenomena.

The Fick's law allows to obtain the diffusion of one substance into another.

$$\vec{f}_D = -\vec{D}\nabla c \tag{2}$$

where $\vec{D} = (D_x, D_y, D_z)$ are the diffusion coefficients in each axis.

The dragging of the fluid by the wind permits to compute the advection component:

$$\vec{f}_A = -c\vec{u} \tag{3}$$

where $\vec{u} = (u_x, u_y, u_z)$ is the wind velocity.

Adding up the two components of f ($\vec{f}_D$ and $\vec{f}_A$), and replacing them into (1) we have:

$$\frac{\partial c}{\partial t} + \nabla \cdot (c\vec{u}) = \nabla \cdot (\vec{D}\nabla c) + s \tag{4}$$

There are two constraints to be considered for solving (4), which are:

- If the z-axis is considered as the ground; the dispersion only happens in $z \geq 0$.
- The concentration tends to 0 when is analyzed in a far field.

Then:

$$u_z c - D_z \frac{\partial c}{\partial z} = 0 \;\; at \;\; z = 0 \tag{5}$$

If we consider $u_z = -u_{set}$ as settling velocity for the particulates and W_{dep} as a deposition coefficient that captures the effect of total flux of contaminants penetrating the ground, we have the Robbin Boundary Condition:

$$-u_{set} c - D_z \frac{\partial c}{\partial z} = -W_{dep} c \tag{6}$$

1) THE SOURCE

A point source models the air pollutant source in space, using a Dirac delta function $\delta(\cdot)$:

$$s(\vec{X}, t) = Q \cdot \delta(x - x_s)\delta(y - y_s)\delta(z - z_s) \tag{7}$$

where $\vec{x}_s = (x_s, y_s, z_s)$ is the source position and $Q[kg/s]$ is the total output of the source per time unit.

2) DIFFUSIVITY COEFFICIENT

The chemical air pollutant considered in this work is sulfur dioxide (SO_2). Burning coal in power plants or petroleum-based products produce this kind of colorless gas. There are several methods to compute the coefficient of the diffusion of one substance into another. This work uses the Fuller method [29]:

$$D_{AB} = \frac{10^{-3} T^{1.75} \left[\frac{1}{M_A} + \frac{1}{M_B}\right]^{1/2}}{P\left[\left(\sum v_A\right)^{1/3} + \left(\sum v_B\right)^{1/3}\right]^2} \tag{8}$$

where:

- T represents the temperature
- P represents the pressure
- M_A, M_B are the molecular weights of A (air) and B (SO_2), respectively
- $\sum v$ represents the Molecular volume of diffusion

Fig. 1 shows a simulation output of the plume distribution for SO_2. The source is located at 3 meters height.

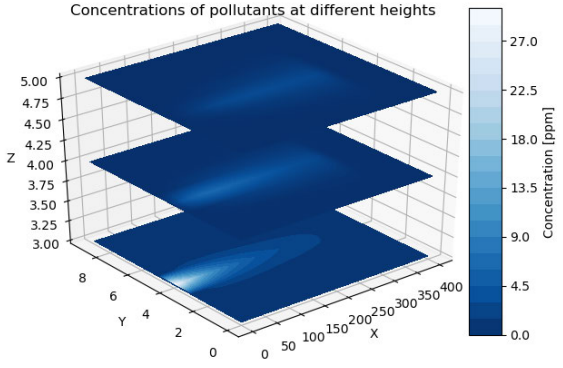

FIGURE 1. Plume shapes at 3, 4 and 5 meters above the ground.

B. SOURCE PROBABILISTIC MAP

The UAVs navigation is performed by using a probabilistic reference map limited to the search area. The probabilistic map is finite and meshed, where every cell (C_{xy}) corresponds to the probability, P_{xy}, of finding the pollutant source at C_{xy}. Fig. 2 shows a layout of a reference map, where it is noticeable that the x-axis grows to the east, while the y-axis to the north. The dimensions of every cell in the map are $L_x \times L_y$. The location of each cell center (on geographical coordinates) is calculated as:

$$center_{Lat}(m) = Lat_L + \frac{Lat_U - Lat_L}{M} \cdot \left(m + \frac{1}{2}\right) \tag{9}$$

$$center_{Lon}(n) = Lon_L + \frac{Lon_U - Lon_L}{N} \cdot \left(n + \frac{1}{2}\right) \tag{10}$$

where:

- m and n are cell indices along y and x axis, respectively
- M and N are the number of cells on the y and x axis, respectively

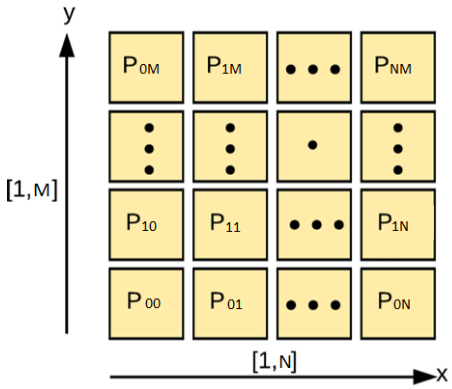

FIGURE 2. Meshed reference map of the quest area.

- Lat_L and Lat_U represent the lower and upper latitude boundaries
- Lon_L and Lon_U represent the lower and upper longitude boundaries

With the previous reference map, it is possible to obtain the probability map. Building this map requires calculating the probability of finding a source in cell C_i (releasing a single chemical filament since time t_l) given that a pollutant chemical is detected (measured) on the cell C_j at time $t_k > t_l$ [30]:

$$S_{ij}(t_k) = \frac{e^{-\frac{(|n_j-n_i|-v_x)^2}{2t_k\sigma_x^2}} e^{-\frac{(|m_j-m_i|-v_y)^2}{2t_k\sigma_y^2}}}{2\pi t_k \sigma_x \sigma_y} L_x L_Y \tag{11}$$

Taking into account that σ_x and σ_y are the variance from a Gaussian distribution (similar to [30]), and that:

$$V(t_l, t_k) = (v_x(t_l, t_k), v_y(t_l, t_k)) = \sum_{i=l}^{k-1} U(X_j(t_i)) \tag{12}$$

where U is a vector with the wind measurements from time t_l to t_k.

By using (11), it is possible to define the probability matrix (or probability map) which implies finding a source in C_i given that a chemical was detected on C_j at time t_k, for all possible release times:

$$\beta_{ij}(t_k) = \frac{S_{ij}(t_{k-1}) + S_{ij}(t_k)}{k} \tag{13}$$

Note that in the previous formulas the i sub-index denotes the source location, and j denotes the current UAV location, on the reference map.

C. SEARCH STRATEGY

All strategies require an initialization process, that is:

1) The MAVLINK controller is created and establishes a communication with the flight controller (Pixhawk or ArduCopter).
2) The reference map (section II-B) is deployed considering one of the UAVs on its center as reference
3) The pollutant plume is linked to the reference map. During experiments, it is located at four different positions: northeast, southeast, southwest, and northeast of the center of the map, keeping their respective locations for the three strategies
4) Both UAVs take off from different (but inside the area) locations

Each strategy has a specific behavior in the exploration and exploitation phases. The exploration phase consists on the period of time where the UAVs search for a high pollutant measurement. The exploitation phase starts after exploration phase has finished (a high pollutant measurement was obtained) and consists on the coordination of each UAV to track the source position.

1) COHERENT EQUIDISTRIBUTED SEARCH WITH PROBABILITY-BASED TRACKING ALGORITHM (CESPT)

The proposed search strategy is able to guide the UAVs to maximize the covering area, using different flight heights for each UAV to avoid collisions during the exploration phase. To this end, two paths are generated by using coordinates points based on Hammersley sequences [31]. A Hammersley sequence of points in a plane has the characteristic of being equidistributed. This characteristic is important to ensure that the UAVs visit places throughout the search area.

Once the Hammersley sequence is generated, the points are scaled according to M and N. Then, the points are split into two groups by means of the k-means clustering algorithm [32], as shown in Fig. 3.

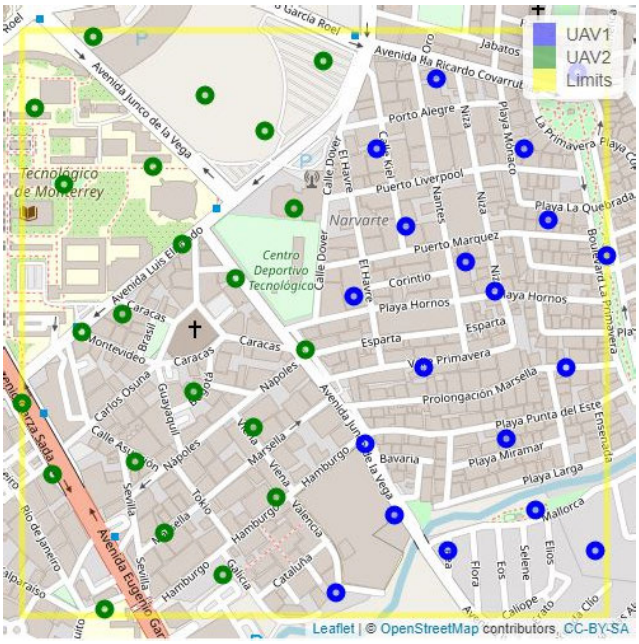

FIGURE 3. Points (based on Hammersley sequences) clustered and located in the search area (500m x 500). Boundaries of the search area are in yellow. Blue points were assigned to UAV1 and green points were assigned to UAV2.

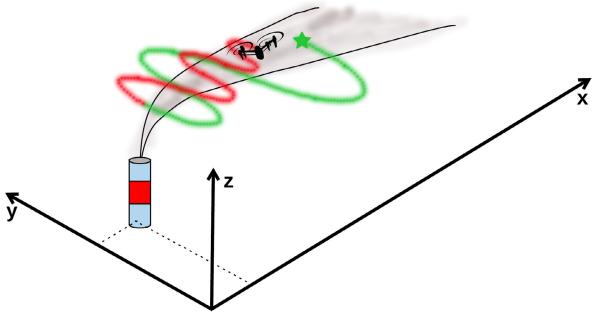

FIGURE 4. Once a high measurement of pollutant is detected, the UAV fly on semicircular trajectories around the plume: against the wind (green trajectory) or downwind (red trajectory). With every high pollutant measurement the circle radius is reduced.

Each group of points will be used to build the paths using a cubic spline planning algorithm [33]. To ensure that each of the resulting paths is smooth, it is necessary to sort the points according to their distance matrix, before applying the path planning algorithm. This situation is solved by using the Traveling Salesman Problem (TSP) solution [34].

To make the UAVs follow their respective path, a proper MAVLINK message should be generated. Firstly, it is necessary to select a type of frame. In this case a global frame with relative altitude is used. The MAVLINK parameter that represents this frame is: MAV_FRAME_GLOBAL_RELATIVE_ALT. Secondly, the mission item command is created with the MAVLINK command MAV_CMD_NAV_WAYPOINT. This command is used to guide the UAV to a specific GPS point and requires the latitude, longitude and altitude of the target location. This location is given by the GPS coordinates of the path previously generated, and a fixed altitude. More information about the MAVLINK commands and parameters can be found on [26] and [35].

The exploration phase ends when a high pollutant level is measured at cell C_k on the reference map. Then, the exploitation phase starts and the probabilistic map (see section II-B) is built considering current value of C_k. In this phase, each UAV follows semicircular trajectories around the points C_{prob} and C_{max}. The point C_{prob} is the position with the highest probability on the probabilistic map. The point C_{max} is located where the highest pollution measure was taken. When the UAV measures a high level of contaminant, both points (C_{prob} and C_{max}) are recalculated, and the semicircle radius and ground-speed of the UAV that sampled the high measure are reduced. Fig. 4 shows an illustrative trajectory followed by a single UAV around a plume.

A simple proportional control allows to generate semicircular trajectories. This control is developed under a North-East-Down (NED) reference frame. The selected MAVLINK parameter for this kind of frame is MAV_FRAME_BODY_NED. With this frame, the x, y and z axis on the NED frame are relative to the current UAV position. In the proportional control the velocity on x (V_x) is fixed and the velocity on y (V_y) is given by:

$$V_y = -O \cdot K_p \cdot e \tag{14}$$

where:

- O is the orientation of the UAV movement ($O = 1$ to clockwise and $O = -1$ to counter-clock wise).
- K_p is the proportional gain of the controller.
- e is the difference between the desired radius of the circular trajectory (R) and the distance from the UAV to the circle center of that trajectory.

Fig. 5 shows a scheme of the previous variables on the circular path control. By using the command message SET_POSITION_TARGET_LOCAL_NED_ENCODE, it is possible to send the desired velocities V_x and V_y to the UAVs, through the MAVLINK protocol.

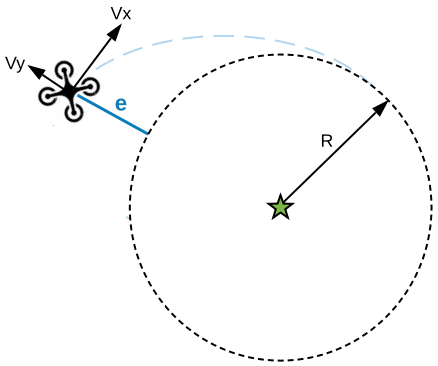

FIGURE 5. Circular path control.

III. EXPERIMENTS AND RESULTS

This section presents a performance comparison of the main approach and the other three strategies based on the algorithms developed in [3], [36]–[39], to locate a pollutant source within a simulated environment.

The simulated environment has the following characteristics:

- The search area has no obstacles for UAVs
- The UAVs autopilot works with the MAVLINK navigation protocol
- The wind measurements were obtained from a real anemometer located at 5 meters height
- The simulation time for each experiment is 10 minutes
- There is only one pollutant source in the search area
- Each UAV flies at different altitude
- The search area is a 500 $m \times 500$ m square
- The minimum detection level is 0.01 [ppm] (given by Official Mexican Standard NOM-038-ECOL-1993, for SO_2). If a sensor measure exceeds this value it is considered as high pollutant concentration measure
- The GPS always delivers good measurements

In order to compare the results of the CESPT strategy (or strategy 1), three other search strategies are simulated. In exploration phase the first strategy to compare (or strategy

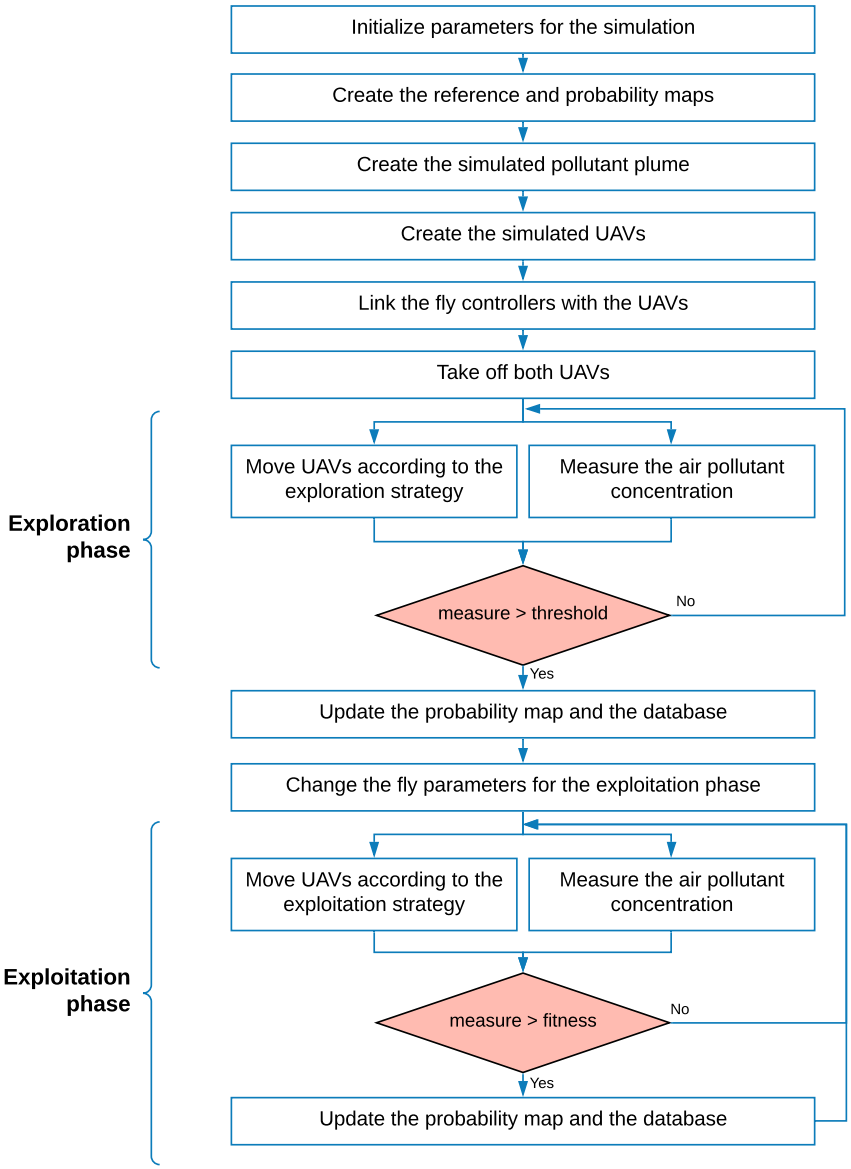

FIGURE 6. Base algorithm used in each strategy.

2) follows circular trajectories around random points on the search area, in a similar way to the work shown in [37]. In exploitation phase a leader-follower behavior is adopted, as is proposed by [38]. On this cooperative formation, the followers fly around the leader in circular trajectories. To achieve this, the ground velocity of the leader is slow and the velocity of the follower is higher. The leader always is flying towards the highest measure detected. The second comparison strategy (or strategy 3) has a random walk behavior in the exploration phase [36]. On the exploitation phase, a Particle Swarm Optimization algorithm is used to guide the UAVs [3]. The third comparison strategy (or strategy 4) consists of a Brownian-like movement, developed by S. Zhang et. al. in [39]. In this work, both phases have similar behavior. The difference for the exploitation phase is a rule that prevents the UAV to select a new fly direction if its current pollutant measure is higher than the previous one. Some modifications were required to adapt the original algorithm to our simulated platform:

1) In the exploration phase the x domain of the search map is divided for each UAV
2) The step of the UAVs is divided in half for the exploitation phase
3) The range of motion for both UAVs is restricted to be one step of the location of the best measurement taken

The base algorithm used with each strategy is showed in the Figure 6. Examples of UAVs flying paths, after each strategy conclusion, are shown in Figures 7, 8, 9, and 10.

A. PERFORMANCE IN EXPLORATION PHASE

The first results to take into account are the amount of high measurements obtained during the exploration phase. In order

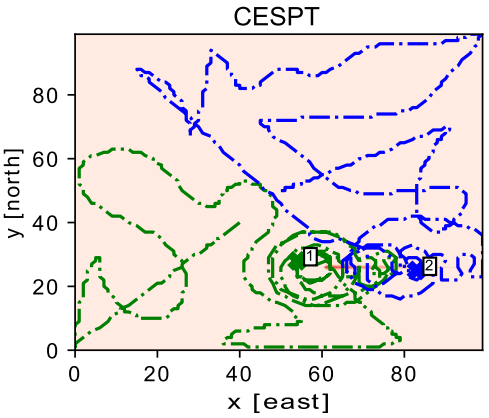

FIGURE 7. Behavior of both UAVs on the reference map, for the CESPT strategy in 10 minutes of flight. Red color represents the pollutant plume, green color represents trajectory of UAV 1, blue color represents trajectory of UAV 2.

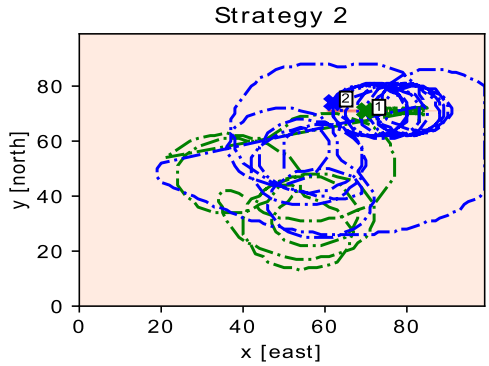

FIGURE 8. Behavior of both UAVs on the reference map, for strategy 2 in 10 minutes of flight.

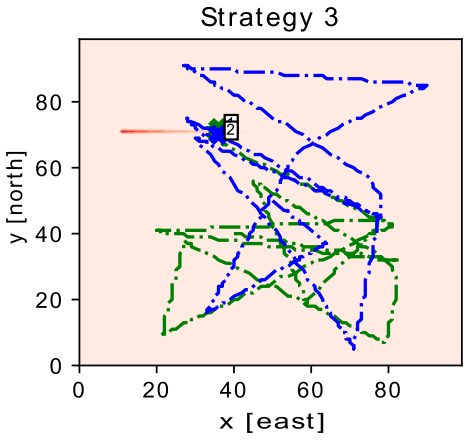

FIGURE 9. Behavior of both UAVs on the reference map, for strategy 3 in 10 minutes of flight.

to verify if there is a difference between the 4 strategies, a Cochran's Q test was developed. The hypothesis on this test are:

- H_0 = All experiments are equally effective.
- H_a = There is a difference in efficacy between experiments.

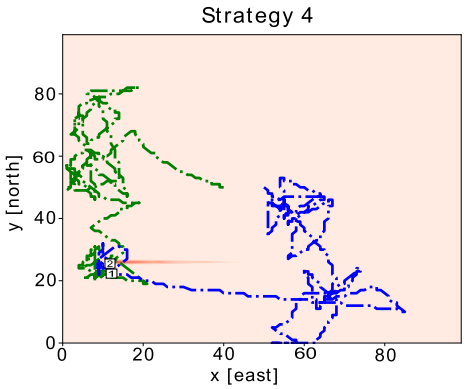

FIGURE 10. Behavior of both UAVs on the reference map, for strategy 4 in 10 minutes of flight.

Each of the 4 strategies was tested 160 times. 80 trials in which the height of one UAV matches the height of the polluting source and 80 with both UAVs flying at a height different from source location. It is considered a detection when a sensor takes a measurement of air pollutant concentration above the minimum detection level previously established (0.01 ppm). The number of detections is shown in Table 1.

TABLE 1. Number of detections per each block based on coincidences with the source height. Match=one UAV flying at source height; No match= both UAVs flying at heights different from source.

	Strategies			
Coincidence	1	2	3	4
Match	75	77	74	49
No match	75	77	77	44
Total of no detections	10	6	9	67

The value of Cochran's chi-squared statistic for the three first results is $Q = 1.1667$. The p-value is 0.558, which indicates that H_0 cannot be rejected. Strategy 4 is not considered because its results are significantly less than the others. Results shown that the 3 first strategies in the exploration phase have equal effectiveness in finding high measurements of pollutant.

We analyze the time required to perform one loop in each strategy for each phase. These results were obtained in a machine running Windows 10 with the processor Intel(R) Core(TM) i7-3610QM (2.30 GHz). The dispersion of the results is shown in the figure 11 and table 2. The graph shows that CESPT needs more time to perform a loop in both phases. That is because this strategy needs to compute a search of the best probability cell, the nearest waypoint in the planned path, and update the probability map. The other strategies are based on random numbers that need fewer operations to be calculated.

Now, an analysis of the time elapsed until the first detection will be performed for each strategy (time to complete

TABLE 2. Statistical values for the time needed to perform a loop by each strategy (in seconds).

	Exploration				Exploitation			
Statistics	1	2	3	4	1	2	3	4
Min	0.224	0.077	0.077	0.0537	0.226	0.08	0.001	0.0537
1st Qu.	0.258	0.0867	0.084	0.0556	0.257	0.087	0.002	0.0547
Median	0.264	0.098	0.095	0.0567	0.264	0.099	0.002	0.0557
Mean	0.278	0.0989	0.0934	0.0595	0.261	0.0996	0.00309	0.0573
3rd Qu.	0.274	0.109	0.098	0.0605	0.27	0.106	0.004	0.0576
Max.	0.657	0.135	0.132	0.131	0.346	0.192	0.034	0.0986
std	0.0536	0.0133	0.00981	0.00831	0.0149	0.0137	0.00276	0.00465

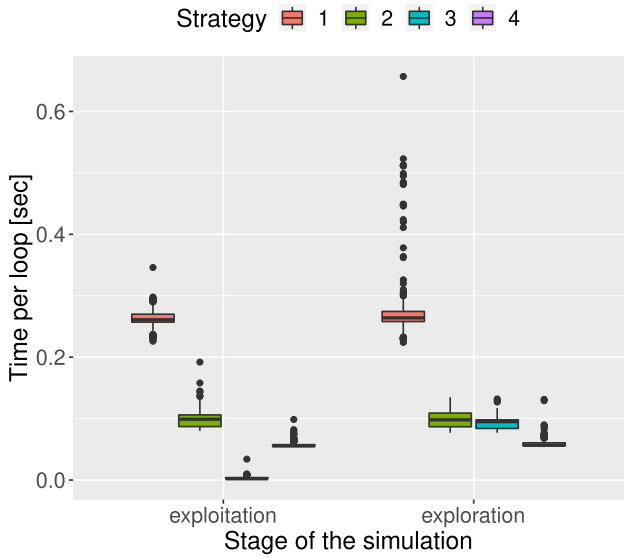

FIGURE 11. Time required to complete one loop by each phase of each strategy.

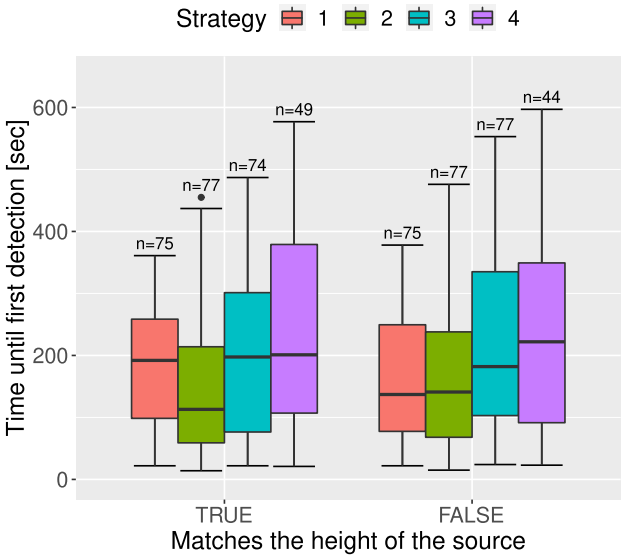

FIGURE 12. Time required to complete the exploration phase of each strategy. "TRUE" are experiments when 1 UAV is flying at the height of the pollutant source. "FALSE" are experiments when none of the UAVs is flying at the pollutant source height.

the exploration phase and start the exploitation phase). This variable is calculated from the time when the UAVs finish their initialization process until the time the first high concentration of pollutant is measured. The results for this variable are summarized on Figure 12. The statistics of this graph are shown in Table 3.

Looking at the box plots, is observed that the second strategy (in matching experiments) need less time to have the first detection. In no matching experiments, strategies 1 and 2 have similar results.

B. PERFORMANCE IN EXPLOITATION PHASE

The main objective of the strategies is to find the location of the pollutant source. The *source_location* response is a couple of GPS coordinates given by the pair (latitude, longitude). Each UAV changes those coordinates during the experiment when a better level of pollutant is measured. Its final value is taken when the flying time is over at 10 mins.

It is important to note that the CESPT strategy delivers 2 types of *source_location* results. The first result corresponds to the deterministic position found by the highest measurement taken by the sensors. The second response is the probable location related with the probabilistic map (shown in section II-B). It correspond to the cell C_i with highest probability, transforming its indices with Equations (9) and (10). So, the first case will be represented as strategy 1 and the second case was labeled as strategy 1.5.

The first performance index to be compared between strategies will be the distance to the pollutant source. This measure is the distance (computed with the Haversine formula, which determines the great-circle distance between two points on a sphere given their longitudes and latitudes) between the *source_location* given by the strategy and the real coordinates of the pollutant source. Figure 13 shows the box plots representing the distribution of these results. The statistical values for these distributions are shown in Table 4.

It is easily notable that the probabilistic part (strategy 1.5) of the strategy 1 results on closer locations to the air pollutant source. The dispersion, represented by the standard deviation

TABLE 3. Statistical values for time until the first detection (in seconds).

	Matching strategies				No-matching strategies			
Statistics	1	2	3	4	1	2	3	4
Min	22	14	22	21	22	15	24	23
1st Qu.	98.5	59	76.5	107	77.5	68	103	91.5
Median	192	113	197.5	201	137	141	182	222
Mean	171.8	143.4	196.6	242	160.9	168.8	216.1	249
3rd Qu.	258.5	214	301.2	379	249.5	238	335	349
Max	361	455	487	577	378	476	553	597
std	96.31	106.09	128.3	164	101.95	120.75	144.22	165

TABLE 4. Statistical values for proximity to the pollutant source (in meters).

	Matching strategies					No-matching strategies				
Statistics	1.5	1	2	3	4	1.5	1	2	3	4
Min	1.42	1.17	1.81	2.74	1.47	1.42	13.41	45.14	3.17	12
1st Qu.	9.09	5.90	16.37	31.85	11.7	11.08	63	70.23	54.19	50.5
Median	14.09	22.51	63.18	71.11	19.1	15.99	74.53	71.67	90.17	76.2
Mean	20.09	38.11	55.71	106.74	35.9	26.39	85.65	85.17	123.09	81.8
3rd Qu.	19.90	71.71	74.86	135.64	44.9	40.96	94.55	79.51	165.83	110
Max	81.21	163.27	182.51	409.13	155	96.04	210.78	160.1	393.73	177
std	18.61	39.19	41.28	100.5	41.8	22.44	39.09	28.41	101.67	47.3

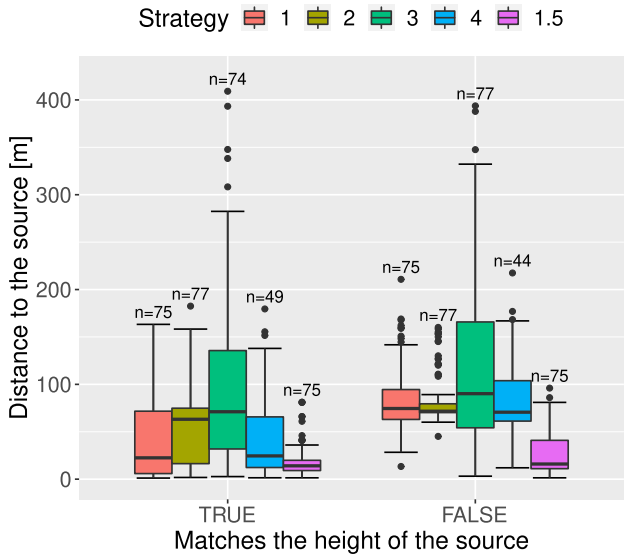

FIGURE 13. Summary of results for the distance to the source.

(std), points to the fact that this strategy will have good performance due to its value is considerably smaller. The second strategy that has good results is the deterministic part of the same strategy 1. If the non match experiments are analyzed, the strategy 1.5 has half of its source proximity results to less than 16 meters. Compared with the rest of strategies with a median greater than 70, it is indisputably that the better response is given by strategy 1.

Another important performance index to be analyzed is the improvement of the results along the experiment. This response corresponds to the difference of the first concentration measure and the last one. These results are shown in Figure 14 and Table 5. This index will show the effectiveness of the algorithms to find higher pollutants concentrations along the time. A small amount of this variable shows that an UAV found a concentration level and was not capable to find better measurements. This behavior could be due to 3 situations:

- The UAV found a very high pollutant concentration in the first measurement
- The UAV found its first good pollutant measurement close to the end of flying time
- The algorithm is not capable to find significantly higher pollutant concentrations

The 3rd strategy has half of their results under 6 ppm. This response shows that the experiments with this strategy fall into one of the 3 previously mentioned situations. With these results it is possible to conclude that the 3rd strategy is the less efficient to find the pollutant source location.

TABLE 5. Statistical values for the improvement of measures (in ppms).

	Matching strategies				No-matching strategies			
Statistics	1	2	3	4	1	2	3	4
Min	0	0.81	0	0	0.03	0.13	0	0
1st Qu.	10.11	11.82	0.01	10	2.68	2.98	0.03	4.11
Median	20.02	17.83	5.61	18.4	4.80	6.13	1.41	5.18
Mean	18.06	17.56	7.37	16.6	4.21	4.86	2.15	4.60
3rd Qu.	26.69	25.05	13.47	24.5	6.18	6.45	3.60	6.06
Max	29.87	29.91	26.09	29.6	6.42	6.46	6.43	6.44
std	9.17	8.45	7.28	9.19	2.01	2.02	2.29	1.95

TABLE 6. Statistical values for highest detection (in ppms).

	Matching strategies				No-matching strategies			
Statistics	1	2	3	4	1	2	3	4
Min	4.17	1.94	0.07	0.722	1.78	1.86	0.03	0.05
1st Qu.	12.06	11.88	1.86	11.4	3.08	5.58	1.43	4.71
Median	21.38	18.78	6.7	20.08	6.37	6.46	2.43	6.11
Mean	20.09	18.56	10.02	18.2	5.23	5.49	3.04	5.28
3rd Qu.	27.85	25.43	16.78	25.1	6.45	6.47	5.85	6.45
Max	29.91	29.91	29.87	29.9	6.47	6.47	6.47	6.47
std	8.39	8.2	8.74	8.81	1.64	1.64	2.34	1.72

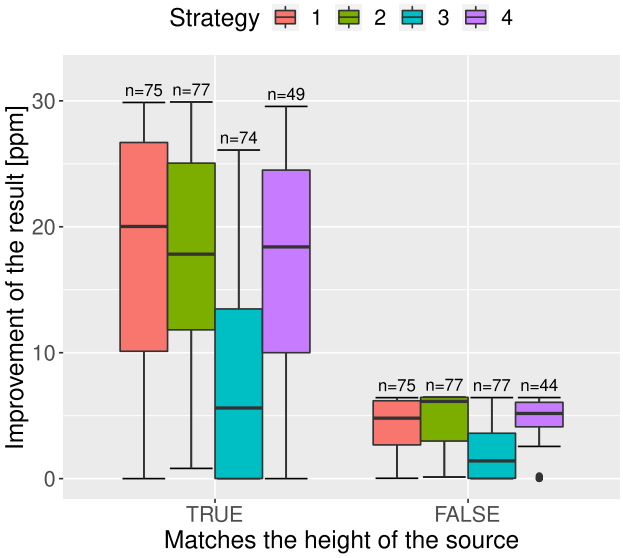

FIGURE 14. Performance of each strategy to find higher levels of pollutant concentration.

FIGURE 15. Highest concentration levels measured.

The last index to be analyzed is the highest measurement taken by the sensors on the UAVs. Figure 15 and Table 6 show how these measurements are dispersed. On first instance a logic supposition is that the distance to the source and the pollutant levels have a negative correlation on all experiments. This supposition is true when the height of the pollutant source matches with the flying height of a UAV, since its correlation index is -0.8. On the other hand, when no UAV flies at the same height of the pollutant source the variables are not correlated. The correlation index on this experiments is -0.15. These results are shown in Figure 16. They explain the good response of the strategy 1, based on

TABLE 7. The planning and control components.

Characteristic	Strategy 1	Strategy 2	Strategy 3	Strategy 4
Exploration paths on the search area	Curved routes based on equidistributed points	Circular routes made at random points	Straight lines to random points	Steps of k meters, based on Brownian motion
Exploitation paths around the detected plume	Semicircular routes around points are obtained deterministically and probabilistically.	The lead UAV flies towards the location with the highest pollutant measure and the follower flies around the leader	Straight lines to points determined by the PSO algorithm	If the measurements increase, the movement is continuous. If not, the UAV moves on steps of $k/2$ meters based on Brownian motion
Median of proximity to the location of the polluting source on matched experiments	**14 m**	63 m	71 m	19 m
Median of proximity to the location of the polluting source on no matched experiments	**16 m**	72 m	90 m	76 m
Median of time until first detection on matched experiments	192 sec	**113 sec**	198 sec	201 sec
Median of time until first detection on no matched experiments	**137 sec**	141 sec	182 sec	222 sec
Median of improvement of measures on matched experiments	**20 ppm**	18 ppm	6 ppm	18 ppm
Median of improvement of measures on no matched experiments	5 ppm	**6 ppm**	1 ppm	5 ppm
Median of highest measures on matched experiments	**21 ppm**	19 ppm	7 ppm	20 ppm
Median of highest measures on no matched experiments	**6 ppm**	**6 ppm**	2 ppm	**6 ppm**

the fact this strategy does not depend only on the pollutant measurements, but in the capability to process information to take good decisions, specially when none of UAVs is flying at the source height.

C. SUMMARY OF RESULTS

After the experiments were performed, it is possible to mention the advantages of using strategy 1.

Advantages:

- The strategy is robust in the scenario where no UAV is flying at the pollutant source height
- The strategy can overcome local maximums
- The exploration phase ensures a distributed route along the search area
- If one UAV fails in the exploitation phase, the other UAV provides a good response, considering as constant previous information (probabilistic or deterministic) of the UAV with faults
- The strategy can be scaled to use more UAVs, considering more probabilistic maps (with different dispersion coefficients for example) or using the second highest contamination measurement

Some disadvantages are mentioned in order to improve the strategy in future works.

Disadvantages:

- The UAVs need more time to follow curves too tight on the exploration phase. This can be addressed by increasing the batteries power or having extra UAVs which take the place of exhausted UAVs.
- If the wind knowledge is not accurate, the probabilistic results will be erratic. This can be amended by including an anemometer in one of the UAVs.

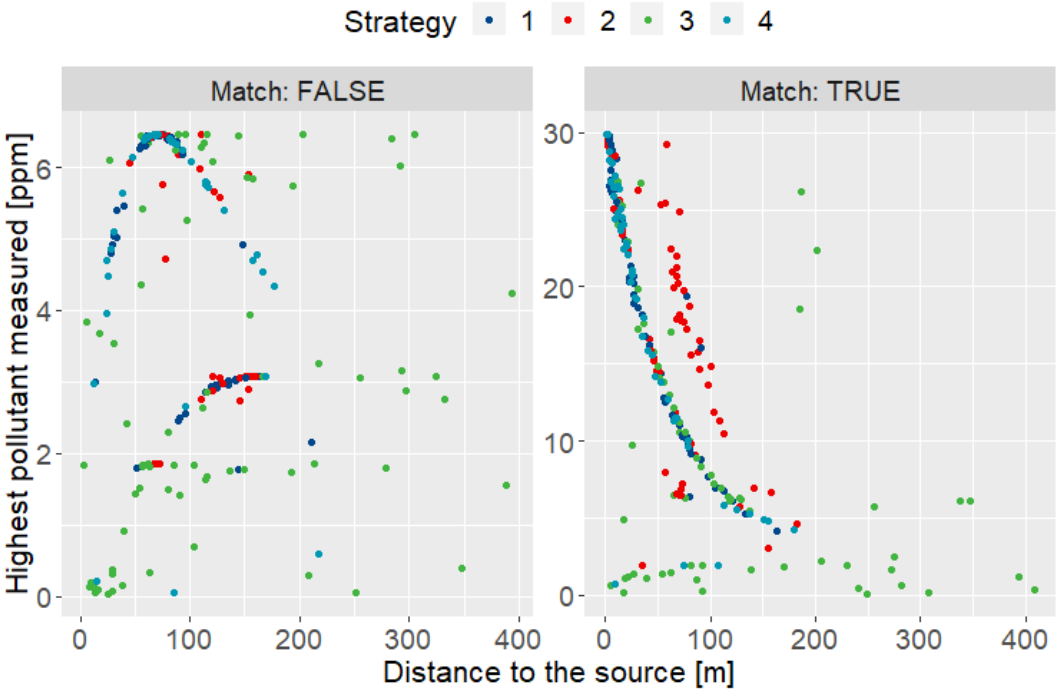

FIGURE 16. Correlation-dispersion diagram between the highest measure of pollutant and the distance to the pollutant source.

Finally, Table 7 shows a summary of the main characteristics of each strategy and the results obtained in the experiments.

IV. CONCLUSION AND FUTURE WORK

In this work we presented an intelligent strategy to locate an air pollutant source on an outdoor area with two UAVs. This strategy was compared against other three in simulated real-time experiments, where a dispersion-advection plume model was used. Unlike previous similar works, our research uses more realistic constraints on the UAVs platform (time of flight, ground speed, sensor sensitivity, communication coverage), in addition to experimenting with a very large search area and initial take-offs from different places. The proposed strategy uses equidistributed search based on Hammersley sequences during the exploration phase. This allows the UAVs to cover different points of the search area, avoiding the repetition of sampling points. Additionally, k-means grouping algorithm, TSP solver and cubic spline algorithms are implemented in this phase to optimize and smooth the navigation. In exploitation phase the information taken by sensors is used to compute the probability of finding the pollutant source and redirect the search to better locations. In this phase semicircular trajectories with decreasing radius are implemented.

The best results of the proposed strategy were obtained in the exploitation stage, showing final locations closer to the source and higher pollutant concentrations.

Future work will focus on implementing other bioinspired algorithms to explore in an efficient way the area. Also, a planning is made to overcome the following disadvantages of the current work: on first instance, is necessary to add a wind model from acquired wind data to strengthen the probability map. The second improvement could be the replacement of the cubic spline with another path tracing algorithm. That algorithm must generate curved paths able to diminish the number of speed reductions in UAVs and increase the chances of having a smoother navigation.

REFERENCES

[1] R.-G. Li and H.-N. Wu, "Multi-robot source location of scalar fields by a novel swarm search mechanism with collision/obstacle avoidance," *IEEE Trans. Intell. Transp. Syst.*, early access, Jul. 28, 2020, doi: 10.1109/TITS.2020.3010056.

[2] Y. Yang, B. Zhang, Q. Feng, H. Cai, M. Jiang, K. Zhou, F. Li, S. Liu, and X. Li, "Towards locating time-varying indoor particle sources: Development of two multi-robot olfaction methods based on whale optimization algorithm," *Building Environ.*, vol. 166, Dec. 2019, Art. no. 106413.

[3] R. Zou, V. Kalivarapu, E. Winer, J. Oliver, and S. Bhattacharya, "Particle swarm optimization-based source seeking," *IEEE Trans. Autom. Sci. Eng.*, vol. 12, no. 3, pp. 865–875, Jul. 2015.

[4] K. Nickels, H. Nguyen, D. Frasch, and T. Davison, "Effective exploration behavior for chemical-sensing robots," *Biomimetics*, vol. 4, no. 4, p. 69, Oct. 2019.

[5] X. Chen and J. Huang, "Combining particle filter algorithm with bio-inspired anemotaxis behavior: A smoke plume tracking method and its robotic experiment validation," *Measurement*, vol. 154, Mar. 2020, Art. no. 107482.

[6] Q. Feng, C. Zhang, J. Lu, H. Cai, Z. Chen, Y. Yang, F. Li, and X. Li, "Source localization in dynamic indoor environments with natural ventilation: An experimental study of a particle swarm optimization-based multi-robot olfaction method," *Building Environ.*, vol. 161, Aug. 2019, Art. no. 106228.

[7] D. Facinelli, M. Larcher, D. Brunelli, and D. Fontanelli, "Cooperative UAVs gas monitoring using distributed consensus," in *Proc. IEEE 43rd Annu. Comput. Softw. Appl. Conf. (COMPSAC)*, Jul. 2019, pp. 463–468.

[8] J. Euler and O. von Stryk, "Optimized vehicle-specific trajectories for cooperative process estimation by sensor-equipped UAVs," in *Proc. IEEE Int. Conf. Robot. Autom. (ICRA)*, May 2017, pp. 3397–3403.
[9] B. Bayat, N. Crasta, A. Crespi, A. M. Pascoal, and A. Ijspeert, "Environmental monitoring using autonomous vehicles: A survey of recent searching techniques," *Current Opinion Biotechnol.*, vol. 45, pp. 76–84, Jun. 2017.
[10] P. Li and H. Duan, "A potential game approach to multiple UAV cooperative search and surveillance," *Aerosp. Sci. Technol.*, vol. 68, pp. 403–415, Sep. 2017.
[11] T. F. Villa, F. Salimi, K. Morton, L. Morawska, and F. Gonzalez, "Development and validation of a UAV based system for air pollution measurements," *Sensors*, vol. 16, no. 12, p. 2202, 2016.
[12] N. Ya'acob, M. Zolkapli, J. Johari, A. L. Yusof, S. S. Sarnin, and A. Z. Asmadinar, "UAV environment monitoring system," in *Proc. Int. Conf. Electr., Electron. Syst. Eng. (ICEESE)*, Nov. 2017, pp. 105–109.
[13] N. M. Yungaicela-Naula, L. E. Garza-Castanón, A. Mendoza-Domınguez, L. I. Minchala-Avila, and L. E. Garza-Elizondo, "Design and implementation of an UAV-based platform for air pollution monitoring and source identification," in *Proc. Congr. Nac. Control Autom.*, 2017, pp. 288–293.
[14] M. Rossi and D. Brunelli, "Autonomous gas detection and mapping with unmanned aerial vehicles," *IEEE Trans. Instrum. Meas.*, vol. 65, no. 4, pp. 765–775, Apr. 2016.
[15] K. Hoshiba, K. Washizaki, M. Wakabayashi, T. Ishiki, M. Kumon, Y. Bando, D. Gabriel, K. Nakadai, and H. Okuno, "Design of UAV-embedded microphone array system for sound source localization in outdoor environments," *Sensors*, vol. 17, no. 11, p. 2535, 2017.
[16] O. Black, J. Chen, A. Scircle, Y. Zhou, and J. V. Cizdziel, "Adaption and use of a quadcopter for targeted sampling of gaseous mercury in the atmosphere," *Environ. Sci. Pollut. Res.*, vol. 25, no. 13, pp. 13195–13202, May 2018.
[17] S. Yang, R. Talbot, M. Frish, L. Golston, N. Aubut, M. Zondlo, C. Gretencord, and J. McSpiritt, "Natural gas fugitive leak detection using an unmanned aerial vehicle: Measurement system description and mass balance approach," *Atmosphere*, vol. 9, no. 10, p. 383, Oct. 2018.
[18] Y. Yang, Z. Zheng, K. Bian, L. Song, and Z. Han, "Real-time profiling of fine-grained air quality index distribution using UAV sensing," *IEEE Internet Things J.*, vol. 5, no. 1, pp. 186–198, Feb. 2018.
[19] R. Kristiansen, E. Oland, and D. Narayanachar, "Operational concepts in UAV formation monitoring of industrial emissions," in *Proc. IEEE 3rd Int. Conf. Cognit. Infocommun.*, Dec. 2012, pp. 339–344.
[20] J. Han, "Small unmanned aircraft systems for cooperative source seeking with fractional order potential fields," in *Proc. Chin. Control Decis. Conf. (CCDC)*, Jun. 2018, pp. 6677–6683.
[21] Z. Fu, Y. Chen, Y. Ding, and D. He, "Pollution source localization based on multi-UAV cooperative communication," *IEEE Access*, vol. 7, pp. 29304–29312, 2019.
[22] A. Marjovi and L. Marques, "Optimal swarm formation for odor plume finding," *IEEE Trans. Cybern.*, vol. 44, no. 12, pp. 2302–2315, Dec. 2014.
[23] V. Šmídl and R. Hofman, "Tracking of atmospheric release of pollution using unmanned aerial vehicles," *Atmos. Environ.*, vol. 67, pp. 425–436, Mar. 2013.
[24] J. Euler, A. Horn, D. Haumann, J. Adamy, and O. V. Stryk, "Cooperative n-boundary tracking in large scale environments," in *Proc. IEEE 9th Int. Conf. Mobile Ad-Hoc Sensor Syst. (MASS)*, Oct. 2012, pp. 1–6.
[25] R.-C. Lee and Y.-H. Chen, "Dual UAV PM2.5 pollution source tracking system," in *Proc. IEEE Eurasia Conf. IoT, Commun. Eng. (ECICE)*, Oct. 2019, pp. 384–386.
[26] A. Koubaa, A. Allouch, M. Alajlan, Y. Javed, A. Belghith, and A. M. Khalgui, "Micro air vehicle link (MAVlink) in a nutshell: A survey," *IEEE Access*, vol. 7, pp. 87658–87680, 2019.
[27] A. Viseras, T. Wiedemann, C. Manss, L. Magel, J. Mueller, D. Shutin, and L. Merino, "Decentralized multi-agent exploration with online-learning of Gaussian processes," in *Proc. IEEE Int. Conf. Robot. Autom. (ICRA)*, May 2016, pp. 4222–4229.
[28] B. Hosseini, "Dispersion of pollutants in the atmosphere: A numerical study," M.S. thesis, Dept. Math. Fac. Sci., Simon Fraser Univ., Burnaby, BC, Canada, 2013.
[29] J. Welty, E. C. Wicks, L. G. Rorrer, and E. R. Wilson, *Fundamentals Momentum, Heat Mass Transfer*. Hoboken, NJ, USA: Wiley, 2007, p. 412.
[30] S. Pang and J. A. Farrell, "Chemical plume source localization," *IEEE Trans. Syst., Man, Cybern. B, Cybern.*, vol. 36, no. 5, pp. 1068–1080, Oct. 2006.
[31] T.-T. Wong, W.-S. Luk, and P.-A. Heng, "Sampling with Hammersley and Halton points," *J. Graph. Tools*, vol. 2, no. 2, pp. 9–24, Jan. 1997.
[32] G. Gan, C. Ma, and J. Wu, *Data Clustering: Theory, Algorithms, Application*. Philadelphia, PA, USA: SIAM, 2020.
[33] L. Nam, L. Huang, X. J. Li, and J. Xu, "An approach for coverage path planning for UAVs," in *Proc. IEEE 14th Int. Workshop Adv. Motion Control (AMC)*, Apr. 2016, pp. 411–416.
[34] D. Davendra, *Traveling Salesman Problem: Theory Application*. Norderstedt, Germany: BoD–Books on Demand, 2010.
[35] Dronecode Project. *Mavlink Common Message Set*. Accessed: Dec. 15, 2020. [Online]. Available: https://mavlink.io/en/messages/common.html#MAV_CMD_NAV_WAYPOINT
[36] J. R. Bourne, E. R. Pardyjak, and K. K. Leang, "Coordinated Bayesian-based bioinspired plume source term estimation and source seeking for mobile robots," *IEEE Trans. Robot.*, vol. 35, no. 4, pp. 967–986, Aug. 2019.
[37] G. Ferri, E. Caselli, V. Mattoli, A. Mondini, B. Mazzolai, and P. Dario, "A biologically-inspired algorithm implemented on a new highly flexible multi-agent platform for gas source localization," in *Proc. 1st IEEE/RAS-EMBS Int. Conf. Biomed. Robot. Biomechatron.*, 2006, pp. 573–578.
[38] S. Zhu, D. Wang, and C. B. Low, "Cooperative control of multiple UAVs for source seeking," *J. Intell. Robot. Syst.*, vol. 70, nos. 1–4, pp. 293–301, 2013.
[39] S. Zhang, Z. Liu, J. Liu, T. Ding, and S. Wei, "Simulation implementation of air pollution traceability algorithm based on unmanned aerial vehicle," in *IOP Conf. Ser., Earth Environ. Sci.*, vol. 675, May 2021, Art. no. 012012.

ANDRÉS F. GARCÍA-CALLE was born in Cuenca, Azuay, Ecuador, in 1993. He received the Engineering degree in electronics and telecommunications from the Universidad de Cuenca, Ecuador, and the M.Sc. degree in sciences of engineering from Tecnologico de Monterey, Monterrey, Mexico, in 2017 and 2019, respectively.

From 2018 to 2019, he was a Research Assistant with the Robotics Laboratory of the Northeast and Central Area of Mexico, Tecnologico de Monterrey. Since 2020, he has been an independent worker focused on data science, optimization, automatic control, and communication protocols.

LUIS E. GARZA-CASTAÑÓN (Member, IEEE) was born in Monclova, Coahuila, Mexico, in 1963. He received the Engineering degree in electronic systems, the M.Sc. degree in control engineering, and the Ph.D. degree in artificial intelligence from Tecnologico de Monterrey, Monterrey, Mexico, in 1986, 1988, and 2001, respectively.

From 1999 to 2003, he was a Lecturer with the Physics Department, Tecnologico de Monterrey. Since 2004, he has been an Associate Professor with the Mechatronics Department, Tecnologico de Monterrey at Monterrey. He is the author of more than 100 articles, chapter books, and books. His research interests include autonomous vehicles, machine learning, fault detection, diagnosis and control, image processing, and advanced control applications.

LUIS I. MINCHALA-AVILA (Senior Member, IEEE) received the B.S.E.E. degree from Salesian Polytechnic University, Cuenca, Ecuador, in 2006, and the M.Sc. and Ph.D. degrees from the Instituto Tecnológico y de Estudios Superiores de Monterrey, Monterrey, Mexico, in 2011 and 2014, respectively. From Summer 2012 to Summer 2013, he was a Visiting Scholar with Concordia University, Montreal, QC, Canada. From 2017 to 2018, he was a Postdoctoral Fellow with the Climate Change Research Group, Tecnologico de Monterrey. He is currently a full-time Researcher with the School of Engineering and Sciences, Tecnologico de Monterrey, Guadalajara, Mexico. He has authored and coauthored over 60 indexed publications, including journal articles, conference proceedings, book chapters, and a book.